Probe-Inspired Nano-Prodrug with Dual-Color Fluorogenic Property Reveals Spatiotemporal Drug Release in Living Cells

Xiangdong Xue, Shubin Jin, Chunqiu Zhang,* Keni Yang, Shuaidong Huo, Fei Chen, Guozhang Zou,* and Xing-Jie Liang*

CAS Key Laboratory for Biological Effects of Nanomaterials & Nanosafety, National Center for Nanoscience and Technology, No. 11 Beiyitiao, Zhongguancun, Beijing 100190, China

ABSTRACT The versatility of the fluorescent probes inspires us to design fluorescently traceable prodrugs, which enables tracking the drug delivery kinetics in living cells. Herein, we constructed a self-indicating nanoprodrug with two fluorescent moieties, an aggregation-induced emission molecule (tetraphenylethylene, TPE) and a luminant anticancer drug (doxorubicin, DOX), with a pH-responsive linker between them. Except when a low pH environment is encountered, an energy-transfer relay (ETR) occurs and inactivates the fluorescence of both, showing a dark background. Otherwise, the ETR would be interrupted and evoke a dual-color fluorogenic process, giving distinct fluorogenic read out. By observing the dual-color fluorogenic scenario, we captured the kinetics of the drug release process in living cells. Because the separated TPE and DOX are both fluorescent but have a distinct spectrum, by examining the spatiotemporal pattern of TPE and DOX, we were able to precisely disclose the drug-releasing site, the releasing time, the destinations of the carriers, and the executing site of the drugs at subcellular level. Furthermore, different intracellular drug release kinetics between free doxorubicin and its nanoformulations were also observed in a real-time manner.

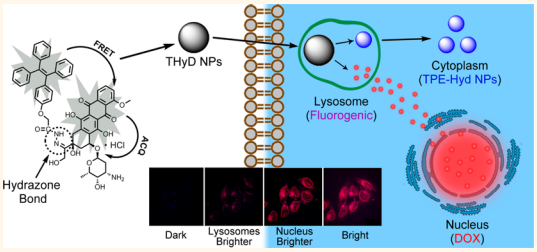

KEYWORDS: dual-color responsive · FRET · aggregation-induced emission · nanoprodrug · pH sensitive

Cells are sophisticated units that implement diverse biological functions by precisely coordinating the activities of different organelles. Each of these subcellular compartments contains a highly specialized microenvironment. To achieve efficient therapeutic effects, nanoscaled drug delivery systems (NDDSs) are usually endowed with stimulus-responsive capacities which allow them to respond to the specific physiological microenvironments within organelles and release drugs at targeting subcellular locations during intracellular trafficking.[1−6] Deciphering these stimulus-responsive drug release kinetics at the subcellular level allows us to understand this process better and control drug release more precisely, thus enhancing the effectiveness of chemotherapeutic agents. However, few studies have provided detailed insight into the kinetics of subcellular spatiotemporal drug delivery *in situ*, particularly in a noninvasive, real-time manner.

In an effort to precisely characterize the nature and location of stimulus-responsive drug release kinetics, fluorescent tags are one of the most powerful tools, as they provide high sensitivity and great versatility while minimally disturbing the cell under investigation.[7−9] Nevertheless, the fluorescent tag may not indicate the actual subcellular location of the NDDSs, as it may be hydrolyzed during intracellular trafficking. Furthermore, some surface fluorescent dye derivatives may alter the physicochemical properties of the NDDSs, causing the tagged NDDSs to have different uptake behaviors from the naked one. To overcome these drawbacks, NDDSs with intrinsic fluorescence, capable of responding to the specific microenvironments within living cells, needs to be developed. Inspired by

* Address correspondence to liangxj@nanoctr.cn, zougz@nanoctr.cn, zhangcq@nanoctr.cn.

Received for review November 17, 2014 and accepted February 17, 2015.

Published online February 17, 2015
10.1021/nn5065452

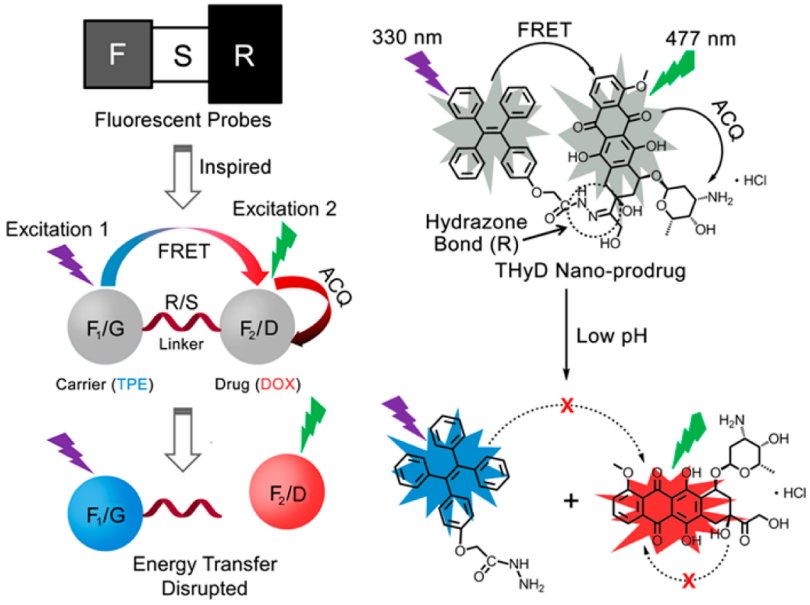

Scheme 1. Schematic illustration of the design of the probe-inspired nano-prodrug. A probe is generally constructed with three parts: F, S, and R units. Between F and R, specific energy transfer (FRET, ICT, PET, *etc.*) determines the fluorescence variations. Based on this, our nano-prodrug was designed using two fluorophore groups with an energy-transfer relay (ETR) scenario; *i.e.*, donor transfers its emissive energy to acceptor, and the acceptor quenches itself by aggregation caused quenching (ACQ). Owing to ETR, the fluorescence of both the donor and acceptor is quenched; once the ETR is disrupted in specific environments, the fluorescence of both F_1 and F_2 reappears. The nano-prodrug is constructed with a guidance molecule (TPE) and drug (DOX), which act as the donor (F_1, TPE) and acceptor (F_2, DOX), respectively. The hydrazone bond is employed as spacer to conjugate TPE and DOX and also acts as the receptor (R) responding to the environmental alteration. Under low pH micro-environment in cells, the hydrazone bond is broken, and the fluorescence of TPE and DOX are both woken up and read out from the dark background. Excitation 1 is 330 nm of TPE, and excitation 2 is 477 nm of DOX. Abbreviations: F, fluorophore group; S, spacer; R, receptor group; G, guidance group; D, drug moiety; THyD, TPE-hydrazone-DOX.

the design concepts of the fluorescent probes,[10−12] we wished to develop a self-indicating nanoprodrug in which dynamic energy-transfer processes, such as fluorescence resonance energy transfer (FRET),[13,14] photoinduced electron transfer (PET),[15−17] or intramolecular charge transfer (ICT),[18−20] occur between the drug and the carrier. When the prodrug is disrupted in specific environments, these energy transfers would be broken, leading to a variation in the fluorescent signal. Hence, we chose a typical fluorescent anticancer drug, doxorubicin hydrochloride (DOX·HCl). But DOX·HCl itself is hydrophilic and will not aggregate into nanoform under physiological conditions. Moreover, DOX is constructed with rigid planar chromophores, which are not easy to assemble into stable nanoparticles.[21−24] To formulate DOX·HCl into a nanoprodrug requires a guiding molecule that meets at least two criteria: (i) it is hydrophobic and (ii) it is capable of forming stable nanoparticles under physiological conditions. This guiding molecule should be able to pair with DOX to form specific energy-transfer relationships. Fluorescent dyes, with intrinsic fluorescent and hydrophobic chromophores, are ideal candidates. However, fluorescent dyes are generally constructed with rigid planar chromophores. Once these dyes are introduced into compact nanostructured drug delivery systems, the fluorescence is greatly reduced by the aggregation-caused quenching (ACQ) phenomenon, which occurs by "$\pi-\pi$ stacking" of the rigid planar chromophores.[25−27] Furthermore, the rigid planar structures also suffer the same assembling problems as DOX. Recently, some self-luminant nanodots with little or no cytotoxicity were fabricated using a special type of fluorescent molecules with aggregation-induced emission (AIE) characteristics.[28,29] Different from the conventional fluorescent dyes, AIE molecules are highly fluorescent in the aggregated state,[30−32] which makes them ideal candidates for self-luminant drug carriers. In our previous work,[33] the AIE molecule, tetraphenylethylene (TPE), could form stable nanoparticles in aqueous solution and display efficient FRET with DOX, allowing them a better fit for the construction of a probe mimetic nanoprodrug. By virtue of the energy transfer between TPE and DOX, *in situ* visualization of the drug release kinetics can be achieved by observing the location and magnitude of the energy-transfer-dependent fluorescence variation.

Hence, as depicted in Scheme 1, we constructed a self-indicating nanoprodrug based on the designing conceptions of fluorescent probes, in which an energy transfer relay (ETR) occurs between two fluorophores (TPE and DOX, corresponding to F_1 and F_2, respectively) and inactivates the fluorescence of both. As we aimed to develop a general conception of designing the self-tracking nanoprodrug to image the intracellular drug release kinetics of NDDSs, we

chose one of the most widely used external-stimulus responsive linkages, a hydrazone bond with a pH-sensitive feature[34,35] that acts as the spacer and receptor group (S/R in Scheme 1) between TPE and DOX. Moreover, the hydrazone bond is a "traceless" reversible chemical bond; the disruption of this bond causes no "pendent" residues remaining on the drug molecules, which permits the precursors returning to their original state from the prodrug form, and allows reproducing the identical intracellular behaviors to the free drugs. Once ETR becomes invalid under low intramolecular pH circumstances, the silenced fluorescence of TPE and DOX is enabled and evokes a dual-color fluorogenic process. By capturing these two color generations, the drug-release kinetics in living cells can be observed.

RESULTS AND DISCUSSION

The prodrug molecules (THyD) were synthesized starting from a TPE precursor we previously reported[33,36] and were conjugated with a commercially available doxorubicin hydrochloride by a hydrazone bond (Figures S1−S5, Supporting Information). Then the prodrug molecules were assembled into nanoparticles that became nanoprodrugs (THyD NPs) by a reprecipitation method.[22,28] As shown in Figure 1a, the hydrophobic TPE moieties successfully guided the assembly of THyD molecules into uniform spherical nanoparticles in normal saline. The size distribution of THyD NPs was around 41 nm (Figure 1b). Next, we examined the ETR-caused dual-fluorescence (FL) quench behaviors in THyD NPs. As shown in Figure 1c,d, the FL of DOX was almost completely quenched upon formation of THyD NPs; this FL quench was ascribed to ACQ. To verify that the ACQ behaviors occurred in THyD NPs, a solvent-dependent aggregation method was employed. The DOX chromophores in THyD molecules showed strong fluorescence at 591 nm when they were dissolved in DMSO, but with the addition of water (normal saline), the fluorescence intensity dramatically decreased (Figure 1e). When the water fraction (f_w, water content in DMSO, vol %) reached 99.9 vol %, the FL intensity of the DOX chromophores was nearly 26.5-fold weaker than that in 100% DMSO (Figure 1f), confirming that the ACQ of the DOX chromophores gradually increased along with the aggregation of THyD. Next we examined the AIE behavior of the TPE chromophores in THy (guidance precursor of THyD). As shown in Figure S9a (Supporting Information), THy was weakly fluorescent when it was dissolved in DMSO, but with the addition of water, the fluorescence (FL) intensity dramatically increased. When the f_w reached 99.9 vol %, the FL intensity of THy was nearly 90-fold stronger than that in 100% DMSO. The quantum yields (ΦF) of THy in DMSO at different water fractions were also measured.[37,38] When f_w was <60%, the quantum yield of THy was very low (ΦF < 0.43%), but when f_w was ≥60%, the

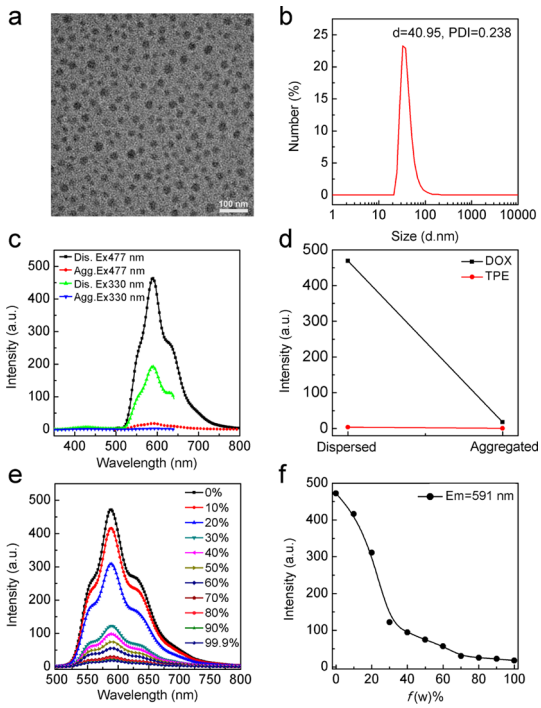

Figure 1. Morphology, size distribution, and the ETR-based dual FL quenching behaviors of DOX and TPE in THyD NPs: (a) morphology of THyD NPs observed by TEM; (b) size distribution of THyD NPs evaluated by DLS; (c) variations of TPE and DOX fluorescence in 50 μM THyD under dispersed (Dis) and aggregated (Agg) conditions; (d) plot calculated from (c) showing the FL quenching behaviors of DOX and TPE. The water fractions were adjusted by using normal saline (0.9% NaCl); (e) aggregation-caused quenching (ACQ) of doxorubicin fluorescence in 50 μM THyD in different fractions of water (f_w) (the f_w means water content in DMSO (percentage in volume)); (f) plot calculated from (e) showing the ACQ behavior of DOX. TPE, excitation/emission, 330/466 nm; DOX, excitation/emission, 477/591 nm.

quantum yield greatly increased, reaching 17.5% when f_w was 99.9%, (Figure S9b, Supporting Information). This suggests that in the presence of a poor solvent (water), the AIE of THy is enhanced because the molecules are increasingly aggregated. The AIE behavior of THy indicates that it is suitable for preparation of self-indicating drug carriers. A similar approach was employed to evaluate the FL behaviors of the TPE chromophores in THyD. As shown in Figure 1c,d, the TPE chromophores showed no obvious FL enhancement in the aggregated state. The AIE behavior of TPE seemed to disappear in THyD NPs. Previously, we reported that TPE and DOX showed an obvious FRET phenomenon,[33,39] as the peak emission wavelength of TPE largely overlaps with the excitation wavelength of DOX (Figure S10, Supporting Information). Thus, in THyD NPs, the disappearance of the AIE behavior of TPE was ascribed to transfer of its emissive energy to DOX. We confirmed that in the THyD NPs, the FL of both TPE and DOX was quenched through ETR, in which the emission from TPE was transferred to DOX, and DOX was self-quenched due to the ACQ phenomenon. As a control, we also conjugated TPE and DOX

with an uncleavable linker (amide bond) and formed TAmD molecules (Figure S6−S8, Supporting Information). Similar ETR caused FL quenching behavior to occur in the control (TAmD NPs). As shown in Figure S11 (Supporting Information), the FL of DOX and TPE were both quenched when TAmD aggregated into nanoparticles. Thus, a dual-fluorescence-quenched THyD and TAmD nanoprodrug was prepared; the FL of both the carrier and drug was "turned off" due to ETR. We hypothesized that in the THyD nanoprodrug the FL of the carrier and drug would be recovered and show a dual-color fluorogenic process once the hydrazone bond recognized the low pH microenvironment in cells and the disrupted ETR reversed fluorescence quench. In contrast, fluorescence "turn on" may not occur in TAmD NPs, as the amide bond is not easily hydrolyzed.

The THyD NPs were designed to respond to the intracellular pH microenvironment in cells and trigger dual-color recovery of TPE and DOX. Hence, the fluorescence of THyD NPs is supposed to be recovered when exposed to acidic intracellular compartments such as lysosomes (pH 5.0), which can break down waste materials and exotic species.[40,41] Therefore, an *in vitro* assay that mimics the intracellular pH of lysosomes was employed to evaluate the dual-color responsiveness of TPE and DOX in THyD NPs. The fluorescence recovery of THyD NPs in different pH conditions was visualized using a UV lamp with an excitation wavelength of 365 nm. As shown in Figure 2a, THy NPs and free DOX both showed strong fluorescence in normal saline at neutral pH. The THyD NPs were fluorescently inactive, indicating that the FL of THy and DOX were both quenched, which is consistent with the FL spectra (Figure 1b,c). As we adjusted the pH of the THyD normal saline suspension to 5.0 with acetic acid, the red fluorescence of DOX recovered, which indicates that the ACQ phenomenon was reduced as some of the DOX was released from the THyD NPs. The FL spectra of THyD NPs under different pH conditions were further evaluated, as shown in Figure 2b. When the pH of the normal saline suspension was adjusted to 5.0, the FL intensity of DOX increased significantly, confirming that DOX was released from THyD NPs. We also tested the TPE FL recovery of the THyD NPs in acidic normal saline; however, no obvious FL recovery was observed, presumably because of the persistence of FRET between the TPE and DOX molecules. Hence, THyD NPs were suspended in acidic normal saline (pH 5.0) and dialyzed in a dialysis bag (MW 3000 Da) for 24 h to separate the detached DOX from THy. The FL behavior of the THy in the dialysis bag was evaluated. As shown in Figure 2c, the FL of THy recovered, indicating that after being detached from DOX the AIE behavior of THy was retained. The fact that THy showed AIE behavior and stayed in the dialysis bag suggests that THy remained in an aggregated state when

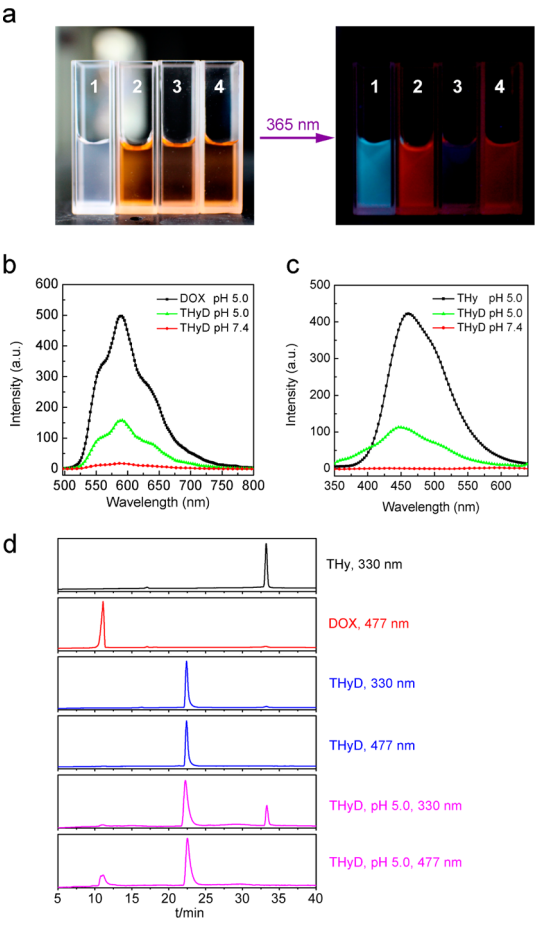

Figure 2. Dual-color responsiveness of THyD when it encounters the low pH circumstcance: (a) pictures of THy (1), DOX (2), THyD (3, neutral pH) and THyD (4, pH 5.0, treated for 24 h) under laboratory lighting (left) and under a UV lamp with laser excitation at 365 nm (right); (b) recovery of DOX fluorescence when THyD was treated with normal saline at pH 5.0 for 24 h; (c) recovery of TPE fluorescence when THyD was treated with normal saline at pH 5.0 for 24 h and the free DOX was removed by dialysis; (d) analyses of the stability of THyD by HPLC. In the experiments, the concentration of ThyD was set at 50 μM. TPE, excitation/emission, 330/466 nm; DOX, excitation/emission, 477/591 nm.

DOX was released from the THyD NPs (Figure S12, Supporting Information). After successfully evaluating the pH-responsive detachment of TPE and DOX by FL assay, we next confirmed that the THyD molecules were hydrolyzed into their original molecular components (THy and DOX). High-performance liquid chromatography (HPLC) was employed to qualify the hydrolysate of THyD. As shown in Figure 2d, THyD gave a single chromatographic peak (retention time: 22.4 min) at neutral pH, indicating that the THyD molecules were intact. After incubation in methanol solution at pH 5.0 for 1 h, THyD gave two additional chromatographic peaks. The retention times of the new peaks (33.3 min at 330 nm, 11.1 min at 477 nm) were identical to THy and DOX, demonstrating that the THyD molecules are able to be hydrolyzed into their original components. The THy molecules kept their structure even after going through the processes of

conjugation with DOX and hydrolyzation from THyD. Furthermore, the released DOX was still in the protonated form, retaining the hydrophilic characteristics that are critical for its biological anticancer activity.[42] Usually, when stimulus-responsive linkers are cleaved under specific biological circumstances, they leave a molecular residue attached to the released drug, which may alter the physicochemical properties and even the pharmacology of the drug. Hence, our design based on hydrazone bond cleavage is a "traceless" reversible disruption, which does not leave any molecular residue on the drug or the carrier after the drug has been released. The fluorescence recovery assay was also performed in the reference system (TAmD), as shown in Figure S13 (Supporting Information). The fluorescence of both TPE and DOX in TAmD NPs was nicely quenched; however, no evidence of TPE FL or DOX FL or disruption of the TAmD NPs was observed, even after treatment with acid. In addition, the HPLC assay did not detect any peaks except for the TAmD chromatographic peak when the control molecules were incubated in acidic methanol solution. We concluded that the TAmD prodrug could not respond to low pH circumstances and released little or no DOX at pH 5.0. Based on the *in vitro* FL recovery evaluation, we hypothesized that THyD NPs would undergo a lysosome-associated dual-color fluorogenic process after being translocated into cells.

After examining the dual-color responsiveness of the THyD and TAmD nanoprodrug *in vitro*, we evaluated their cytotoxicity. MCF-7 human breast cancer cells were treated with free DOX, THyD NPs, and TAmD NPs for 24 h. TCa NPs (carboxylated TPE) and THy NPs were also included as controls to rule out nonspecific toxicity of free TPE molecules. According to the cell viability results shown in Figure S14 (Supporting Information), both DOX and THyD were cytotoxic toward MCF-7 cells after 24 h treatment. The half-maximal inhibitory concentration (IC_{50}) of THyD was 3.96 μM, about 2.5 times that of DOX (1.59 μM). This difference was assumed to result from the delayed release of DOX from THyD NPs in cells, whereas free DOX entered cells directly through diffusion. In contrast, TAmD NPs hardly showed any toxicity to cancer cells because the DOX could not be released. This evidence further supported that the amide bond could not be disrupted in cells. THy NPs and TCa NPs also showed no toxicity, indicating that TPE is safe to cells and the toxicity of THyD was due to the released DOX.

Based on the cell viability results, we hypothesized that the differential cytotoxicity of THyD and TAmD was due to the different pH responsiveness of the hydrazone and amide bonds. Hydrazone bonds are much more labile under low pH condition than amide bonds and would therefore readily release DOX in the acidic lysosomes. According to the fluorescence energy flow, the fluorogenic activities of TPE and

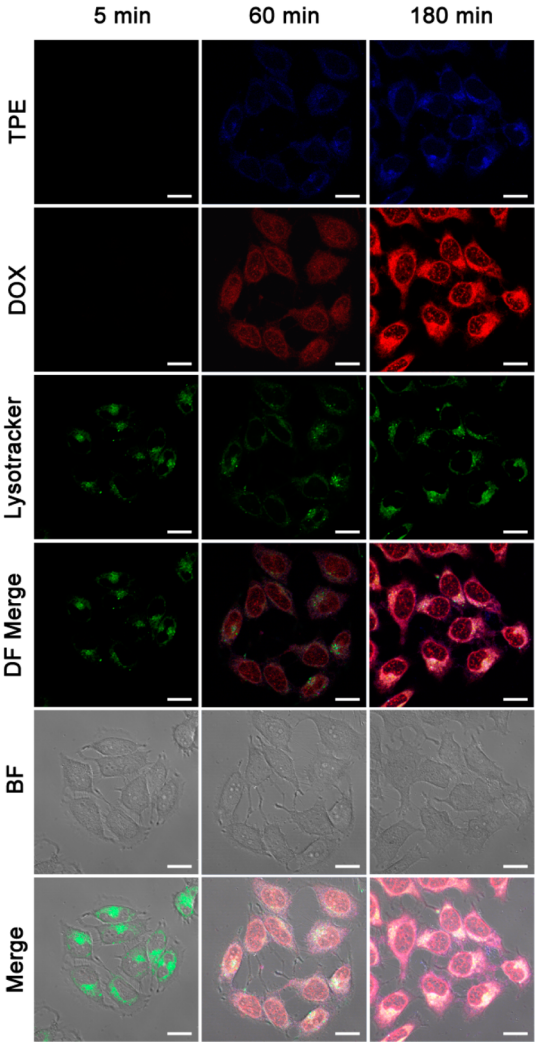

Figure 3. CLSM images depicting the subcellular distributions of THyD NPs in the MCF-7 cell line; the incubation times were 5, 60, and 180 min. Lysosomes were labeled with LysoTracker Deep Red. Scale bar is 20 μm.

DOX will only be observed after the cleavage of linker bonds and disassembly of the nanostructures. The drug release kinetics can therefore be monitored by observing the fluorescence of TPE and DOX in our probes-inspired nanoprodrug. Confocal laser scanning microscopy (CLSM) was then conducted to prove this hypothesis. MCF-7 cells were treated with THyD and TAmD for 5, 60, and 180 min before imaging. As shown in Figure 3, THyD-treated cells exhibited distinct TPE and DOX fluorescence after 180 min treatment and the fluorescence intensity increased with incubation time, suggesting that the drug was successfully released from the THyD NPs in a time-dependent manner. The "blue" fluorescence of TPE was localized in the cytoplasm, in the same location as THy NPs (Figure S15, Supporting Information). No TPE signal was observed in the nucleus, indicating that the carrier just performs its delivery function and does not influence the anticancer effect of the drug. In the "red" fluorescence channel, DOX was distributed in both the cytoplasm

and nucleus. Every cell contained a large cytoplasmic region which showed a particularly strong FL signal from both TPE and DOX. We hypothesized that this region corresponded to lysosomes, where detachment of DOX from the THyD NPs led to a fluorogenic response. To test this, we stained lysosomes with LysoTracker Deep Red (Figure 3, dark field merge) and found that the strong TPE and DOX signals did indeed colocalize with lysosomes. These results supported that the THyD NPs were response to low pH value, and TPE and DOX were released in lysosomes. To disclose the drug release kinetics more precisely, we increased the cellular incubation time with THyD NPs. The MCF-7 cells were incubated with THyD for 6, 12, and 24 h, respectively (The cells were treated with THyD NPs for 3 h, and then the THyD contained medium was replaced with fresh cell culture medium for another 3, 9, and 21 h incubation.) The cells were examined with CLSM (Figure S16, Supporting Information). In 6 h incubation, the fluorescence of TPE and DOX was mostly colocalized in lysosomes, and some DOX entered the nucleus; for a longer 12 h incubation, the subcellular distributions of TPE and DOX remained nearly unchanged compared with the fluorescence distribution of 6 h, but the fluorescence of TPE and DOX became brighter; after 24 h incubation, TPE and DOX mostly distributed in the cytoplasm and perinuclear region, and some of the DOX fluorescence signal was shown in the nucleus. The amount of TPE and DOX colocalized in lysosomes was clearly reduced, and the cells were almost dead (see the bright field, Figure S16, Supporting Information), because most of the cells became round-shaped and floated in the cell culture medium (we also prolonged the incubation time to 48 h, and the cells were all dead). Meanwhile, we observed a signal reduction of LysoTracker in 24 h incubation. We assumed that it was a sign of pH increase which was caused by the continuous proton consumption during the hydrolysis of THyD. From these results, we concluded that the THyD NPs showed a sustained drug-releasing pattern; they released DOX slowly and persistently. As control experiment, we employed another DOX formulation we reported before,[33] *i.e.*, TPE and DOX coprecipitation nanoparticles (TD NPs). In TD NPs, the TPE NPs carried the DOX by electrostatic interaction. The cells were treated with the TD NPs identical to how the cells were treated with the THyD NPs, and the CLSM results are shown in Figure S17 (Supporting Information). The drug release process of TD NPs was much quicker; in 3 h, part of the DOX entered nucleus, and the rest colocalized with TPE in lysosomes and cytoplasm. In 6 h, TPE NPs mostly localized in lysosomes, and the rest distributed in cytoplasm; DOX mostly localized in nucleus, and some of the DOX colocalized with TPE in lysosomes. It indicated that the electrostatic interaction between the TPE and DOX was more liable to be disrupted in the acidic lysosomes and release the DOX quicker. In conclusion, our THyD nanoprodrug experienced a sustained drug release process, the THy NPs finally distributed in the cytoplasm and lysosomes, and DOX localized in the cytoplasm, nucleus, and lysosomes. In comparison, the TD NPs released drugs in lysosomes at a much faster rate. Both nano drug delivery systems were retained in lysosomes and release the drugs, and then the drugs entered the nucleus and TPE carriers stayed in lysosomes or distributed in the cytoplasm. In the control experiment using control nanoprodrug (TAmD NPs), negligible DOX or TPE fluorescence was recovered after 180 min treatment and showed no lysosomes colocalization (Figure S18, Supporting Information). The fluorescence intensity of DOX in cells treated with TAmD for 180 min was even lower than that in cells treated with THyD for 60 min. This result further proved our hypothesis that the amide bond was stable at physiological pH and the DOX cannot be released in cells. Combining the cell viability results, TAmD NPs showed no toxicity to cells after 24 h treatment, which implied that even the incubation time was prolonged and the DOX would not release effectively in TAmD NPs. Therefore, THyD NPs would be employed for real-time visualization of the spatiotemporal pattern of drug release kinetics.

Real-time visualization of spatiotemporal drug release kinetics will enable us to understand this process better and will enlighten future design of sophisticated DDSs. Our THyD NPs are well-suited to this purpose for two reasons. First, all of the fluorescence is eliminated because of the ETR. This means that background noise is removed. Second, these NPs respond to physiological pH changes. Acidic conditions induce a dual-color fluorogenic response from both TPE and DOX once the DOX is released. We have called this response "from darkness to brightness". In order to visualize the spatiotemporal drug release of THyD at the subcellular level and to observe small changes at each time point during this subtle process, we used a real-time CLSM system equipped with a continuous shooting apparatus. This permits a more accurate visualization of the intracellular drug release process during DDS trafficking in living cells. The method is noninvasive because neither cell disruption nor organelle isolation is required. Therefore, MCF-7 cells were incubated with THyD NPs and filmed with real-time CLSM to observe the dual-color fluorogenic activities of TPE and DOX. The cells were treated with THyD NPs for 150 min, and snapshots were captured every 3 min. According to the results (Figure 4 and Figure S19, Supporting Information), an obvious "from darkness to brightness" phenomenon was visualized. During the first few minutes, TPE and DOX were both kept "silent", and the visual field of the CLSM images remained dark. The dark background indicated that our THyD NPs were stable enough to remain quenched in the cell culture

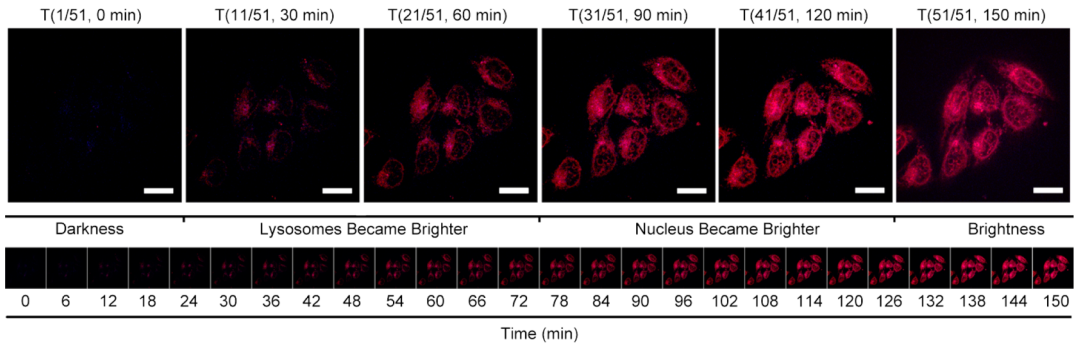

Figure 4. Real-time visualization of the spatiotemporal pattern of drug release by filming the fluorogenic process of the THyD nanoprodrug. The "from darkness to brightness" images were taken every 3 min for a total of 150 min with a PerkinElmer UltraVIEW Vox spinning disk confocal microscope and processed with Volocity software. MCF-7 cells were treated with culture medium containing 50 μM THyD. Before the first snapshot was acquired, 5 min dead time was taken for sample preparation.

medium and suitable for *in vitro* real-time visualization of intracellular stimulus-triggered drug release. Following the transitory period of darkness, the areas containing lysosomes became bright and showed a "purple" color (caused by merging of "red" and "blue" colors), indicating that TPE and DOX were both "woken up", and the fluorogenic process was evoked due to the disruption of THyD NPs. After that, the cell nucleus became bright, indicating that DOX had entered its site of action. By combining all these snapshots together, a vivid spatiotemporal drug release kinetics scenario was depicted. THyD NPs were taken up into cells and translocated into lysosomes. Inside the lysosomes, due to the acidic pH, the hydrazone bonds began to break, the ETR between DOX and TPE was interrupted, and the "silenced" fluorescence began to "wake up" and light up the lysosomes. Then, free DOX invaded the nucleus and executed its antitumor function (see movie 1, Supporting Information). In an effort to elucidate the spatiotemporal drug release process more precisely, we evaluated the variation in fluorescence with incubation time. Figure 5 shows the dual-color fluorogenic process (I/I_0) of DOX and TPE in subcellular organelles (see the regions of interest, ROI) with elapsed time. DOX fluorescence steadily increased in both lysosomes and nuclei; the FL intensity of DOX was enhanced nearly 10-fold after cells were incubated with THyD NPs cells for 150 min, which illustrated the distinct fluorogenic properties of our nanoprodrug. Before 90 min, more DOX was present in the lysosomes than in the nucleus. From 90 min onward, the DOX fluorescence enhancements in the nucleus were higher than that in the lysosomes. The transition point at which more free DOX was present in the nucleus than in the lysosomes is shown in Figure 5. The fluorescence recovery of TPE was also enhanced in lysosomes as the drug was released. In the nucleus, however, the fluorescence of TPE showed no obvious enhancement, which is in agreement with the results shown in Figure 3 and Figure S15 (Supporting Information). When its carrier mission was finished, TPE stayed in the lysosomes or cytoplasm and was unable

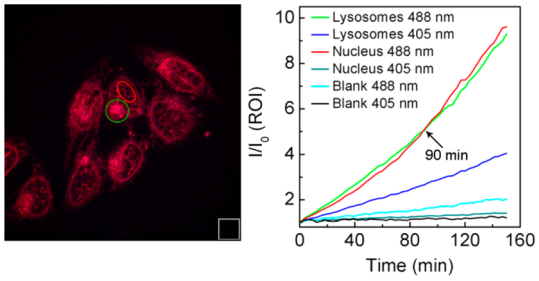

Figure 5. Spatiotemporal distribution of DOX and TPE elucidated by means of the increments of DOX and TPE fluorescence intensity (I/I_0) in three different regions of interest (ROI) as a function of irradiation time (min). The arrow indicates the time when DOX fluorescence in the nucleus is higher than in the lysosomes. On the CSLM image, the green circle outlines the lysosome-rich region; the red oval surrounds part of the nucleus and the white box shows the blank (extracellular) region.

to invade the nucleus and influence the antitumor activities of DOX. The FL enhancement was also evaluated in an extracellular region (blank, cell culture medium, Figure 5). Outside the cells, both TPE and DOX showed no obvious fluorogenic response, which indicated that the THyD NPs were stable enough to remain silent until they encountered the acidic environment in lysosomes. According to the real-time CLSM results, the THyD NPs performed in a lysosome-dependent manner. THyD NPs were first translocated into lysosomes and released the drugs, and then TPE stayed in the lysosomes or diffused to cytoplasm whereas DOX entered the nucleus and performed its antitumor duty. As a control, the cellular uptake of free DOX was also recorded by real-time CLSM. As shown in Figure S20 and movie 2 (Supporting Information), DOX is rapidly taken up into cells and shows no obvious lysosome-dependent translocation behavior. Free DOX seems to directly enter into the nucleus from the cytoplasm. Meanwhile, because of the intrinsic fluorescence of DOX, the red fluorescence spread across the whole visual field, indicating that the fluorescence of free DOX is always "ON" and cannot be switched "from darkness to brightness". By observing the fluorescence of DOX, the nanoprodrug seems to

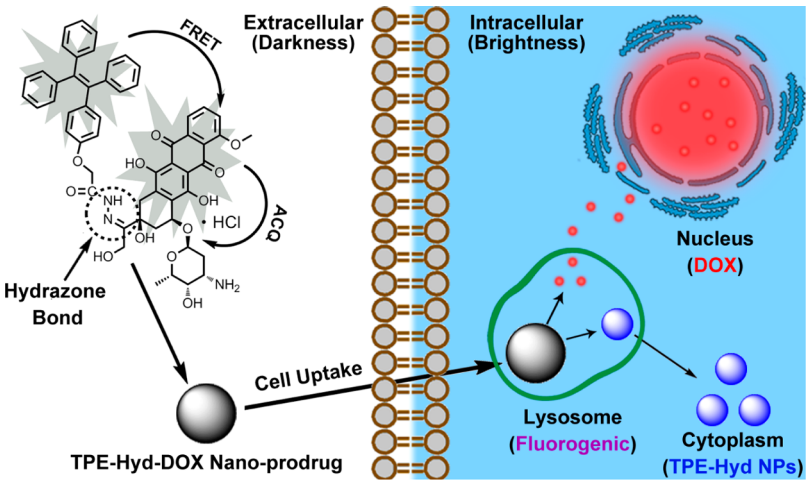

Figure 6. Intracellular trajectory of NDDSs in living cells, which disclosed the trafficking of our probes-inspired nanoprodrug. The nanoprodrug, THyD NPs, fabricated with two fluorophore groups (TPE and DOX) and conjugated with a pH responsive hydrazone bond. In THyD NPs, the ETR effect, mediated by FRET and ACQ, inactivates the fluorescence of TPE and DOX and forms a silent nanoprodrug. By observing the dual-color responsiveness of TPE and DOX, we can observe the following: THyD NPs were first translocated into lysosomes, the drugs were released, and then TPE stayed in the lysosomes or diffused to the cytoplasm, whereas DOX entered the nucleus and performed its antitumor duty.

experience an endocytosis cell uptake pathway and go through a lysosome-associated process, which shares the common uptake mechanism of most nanoparticles when incubated with cells.[43−45] In contrast, free DOX is most likely to enter cells though diffusion, displaying no lysosome-dependent trafficking pattern, but directly invading the nucleus from cytoplasm at a faster speed.

CONCLUSION

The aim of this work was to develop a self-tracking nanoprodrug for noninvasive real-time visualization of the pharmacokinetic and biodistributional behaviors of drugs and carriers *in situ* and, therefore, provide detailed intracellular drug release kinetics information for designing more sophisticated DDSs and improving targeting efficiency of drug to pathological sites. By applying our nanoprodrug to living cells, the intracellular drug trafficking map of pH-responsive DDSs was vividly drawn, as shown in Figure 6, and the nanoprodrug THyD NPs, fabricated with a self-indicating nanocarrier and an anticancer drug with intrinsic luminance, showed excellent theranostic characteristics. The ETR effect, which is mediated by FRET and ACQ, inactivates the fluorescence of THyD NPs. Once ETR was broken by an external stimulus, the fluorescence of TPE and DOX was reactivated, and their specific subcellular locations of the drug and carrier could be monitored. By observing the scenario of the fluorescence recovery, the THyD nanoprodrug platform not only provides a straightforward integration mode of imaging and treatment but also bestows several striking visualization characteristics: (i) the kinetics of the drug release process is captured in a real time, noninvasive manner; (ii) the drug-releasing site (lysosomes) can be visualized, precisely at the subcellular level; (iii) the releasing time and (iv) the destination of the carriers (in the cytoplasm) can be determined; (v) the executing sites of the drugs (in the nucleus) can be disclosed.

In this work, AIE molecules were employed as the drug carriers, which endows the nanoprodrug with better imaging merits: (i) AIE molecules aggregate into self-luminescent nanocarriers, which enable label-free imaging. The fluorescent tags can also make nanocarriers luminescence but need extra chemical modification steps. Furthermore, the fluorescent tags may be hydrolyzed and detached from the carriers during intracellular trafficking and give faulty subcellular location of the carriers. Moreover, some surface fluorescent dye derivatives may alter the physicochemical properties of the nanocarriers, causing the tagged nanocarriers to have uptake behaviors different from those of the naked one. (ii) AIE molecules become fluorescent upon aggregation; their fluorescence variation can disclose whether they are aggregated or not. (iii) The AIE molecules we employed are highly hydrophobic and also act as the guiding molecules to make hydrophilic doxorubicin hydrochloride assemble into nanoparticles. Between the doxorubicin hydrochloride and AIE molecules, the hydrazone bond was employed, which is a "traceless" reversible chemical bond and reveals the drugs release without changing the original structure, which allows our prodrugs to reproduce the identical intracellular behavior to the free drugs. FRET-caused fluorescence increase or decrease between the donor and acceptor is a useful tool to observe the drug release. Because of the energy transfer relay *via* FRET and ACQ, our THyD NPs remained in "darkness" before they released the drugs. When they encountered the specific low pH subcellular environment, a dual-fluorescence fluorogenic process was evoked, and by observing double-color recovery, merging and

separation, we were able to disclose the intracellular drug release kinetics in a more detailed way. Moreover, owing to the FRET and ACQ, the THyD NPs showed a black background in confocal imaging, which allowed us to capture a "from darkness to brightness" scenario and observe the drug release kinetics in a real-time manner.

We also measured the drug release kinetics of different DOX formulations. The hydrazone bond composed nanoprodrug (THyD NPs) experienced a sustained drug release process in lysosomes and released DOX slowly and persistently; the electrostatic interaction composed nanoparticles (TD NPs) released drugs in lysosomes with a faster speed; the amide bond composed nanoprodrug (TAmD NPs) cannot release the drug effectively; and the free DOX was most likely to enter cells through diffusion and directly invade the nucleus from the cytoplasm without being postponed in lysosomes. In addition, our probes-inspired nanoprodrug provided an exciting design that can be used to explore the intracellular drug release kinetics of other stimulus-responsive DDSs, given that the receptor group (hydrazone bond in this research) can be altered to other cellular microenvironments responsive to chemical bonds.

EXPERIMENTAL SECTION

Methods. Unless otherwise stated, all reagents were purchased from commercial suppliers and used without further purification. Water was purified using a Milli-Q system (Millipore, Milford, MA). UV absorbance was tested by an ultraviolet and visible spectrophotometer (Lambda 950, PerkinElmer). Fluorescence was tested by a fluorescence spectrophotometer (LS55, PerkinElmer). Morphology of nanoparticles was evaluated by transmission electron microscopy (TEM, HT7700, Hitachi). Size distributions of nanoparticles were characterized by dynamic light scattering (DLS, Zetasizer Nano ZS, Malvern). The characteristics of each compound were determined by electrospray ionization mass spectrometry (ESI-MS, Amazon SL, Bruker Dalton), matrix-assisted laser desorption ionization time-of-flight mass spectrometry (MALDI-TOF MS, Microflex LRF, Bruker Dalton), nuclear magnetic resonance (NMR, AVANCE III, Bruker Biospin), and high-performance liquid chromatography (HPLC, Waters 2796 with a Waters 2996 PDA detector). The synthesized compounds were purified by pre-HPLC (2535 Quaternary Gradient Module equipped with a Waters 2489 UV/vis detector and Fraction Collector III). MTT evaluation employed a microplate reader (Infinite M200, Tecan). Confocal images were captured by a confocal laser scanning microscopy (CLSM, LSM710, Carl Zeiss). Real-time confocal movies were shot with a spinning disk confocal microscope system (UltraVIEW VoX, PerkinElmer).

Synthesis of 2-[4-(1,2,2-Triphenyl-1-ethenyl)phenyloxy]acetic Acid (TPE-COOH). *Preparation of 1,1,2-Triphenyl-2-(p-methoxyphenyl)-ethene.* Benzophenone (3.68 g, 20 mmol), 4-methoxybenzophenone (4.28 g, 20 mmol), and zinc powder (19.3 g, 100 mmol) were added to a three-necked flask, which was then vacuum-evacuated and flushed 3× with dry nitrogen. A 200 mL portion of dry THF was added, and then $TiCl_4$ (6.8 mL, 60 mmol) was added dropwise using a syringe at 0 °C. After refluxing overnight, the reaction was quenched by addition of 10% K_2CO_3 solution (13.8 g in 125 mL water). The organic phase was washed 2× with brine and then dried over anhydrous $MgSO_4$. The crude product was filtered, concentrated, and passed through a silica gel column with an eluent of petroleum ether and ethyl acetate (20:1 v/v). The final product was a white solid with a yield of 42%.

Preparation of Methyl 2-[4-(1,2,2-Triphenyl-1-ethenyl)-phenyloxy]acetate. A two-necked flask containing 1,1,2-triphenyl-2-(*p*-methoxyphenyl)ethene (3.63 g, 10 mmol) and dried CH_2Cl_2 (100 mL) was cooled to −20 °C, and 2.0 mL of BBr_3 was slowly added. The mixture was warmed to room temperature, allowed to stand for 4 h, and then poured into saturated aqueous sodium bicarbonate. The organic phase was dried over anhydrous $MgSO_4$, and the crude product obtained after concentration was dissolved in 50 mL of CH_3CN. K_2CO_3 (1.38 g, 10 mmol) and methyl bromoacetate (1.0 mL, 10 mmol) were added, and the mixture was refluxed for 4 h before cooling and filtering. The filtrate was concentrated and purified on a silica gel column with an eluent of petroleum ether and ethyl acetate (10:1 v/v) to give 3.54 g of product (82% yield).

Preparation of 2-[4-(1,2,2-Triphenyl-1-ethenyl)phenyloxy]-acetic Acid (TPE-COOH). Methyl 2-[4-(1,2,2-triphenyl-1-ethenyl) phenyloxy]acetate (2.00 g, 4.6 mmol) was dissolved in 150 mL of THF/H_2O (v/v = 7:1). LiOH (1.2 g, 50 mmol) was then slowly added, and the mixture was stirred overnight. THF was removed under reduced pressure and the mixture extracted 3× with 30 mL of CH_2Cl_2. Saturated NH_4Cl solution was added to neutralize the aqueous phase, and the pH was adjusted to 1.0 with 1 M HCl before extracting 3× with 40 mL of ethyl acetate. The organic phase was dried over anhydrous $MgSO_4$ and then concentrated to give TPE-COOH (1.52 g, 81% yield). The NMR spectrum of TPE-COOH is shown in Figure S1 (Supporting Information).

Synthesis of TAmD. TPE-COOH (40.6 mg, 0.1 mmol) was dissolved in 200 μL of DMF solution containing 0.1 mmol of HATU, and then 32 μL of DIEA (0.2 mmol) was added and the solution thoroughly mixed. Doxorubicin hydrochloride (87 mg, 0.15 mmol) was added, and the mixture was stirred at ambient temperature for 2 h. After synthesis, pre-HPLC was employed to purify the product. The desired HPLC fractions were collected and lyophilized, giving about 41 mg of TAmD (43% yield).

Syntheses of THy. TPE-COOH (81.2 mg, 0.2 mmol) was dissolved into 400 μL of DMF containing 0.2 mmol of HATU, then 64 μL of DIEA (0.4 mmol) was added. After thorough mixing, 76.2 mg of Fmoc-Hyd (0.3 mmol) and 4.8 mg DMAP (0.04 mmol) were added. The reaction system was constantly stirred at ambient temperature for 2 h. Piperidine (116 μL, 20% volume ratio to the reaction solution) was introduced into the reaction system and stirred for 30 min at ambient temperature to deprotect the Fmoc residue. The reaction mixture was then purified by pre-HPLC, and around 56 mg of THy was obtained (67% yield).

Synthesis of THyD. THy (42 mg, 0.1 mmol) and doxorubicin hydrochloride (87 mg, 0.15 mmol) were dissolved in 20 mL of anhydrous methanol. The mixture was reacted in the presence of a drop of TFA at ambient temperature for 48 h. After the synthesis, pre-HPLC was employed for purification, and about 36 mg of THyD was obtained (36% yield).

Fabrication of TCa, THy, THyD, and TAmD Nanoparticles. TCa (carboxylated TPE, TPE-COOH), THy, THyD, and TAmD molecules were dissolved in DMSO at a concentration of 100 mM, and 0.5 μL of each solution was added to 1 mL of normal saline with sonication. After the solution was fully vortexed, TCa, THy, THyD, and TAmD NPs were self-assembled.

Fabrication of the TD NPs. TD NPs were fabricated by dropping TPE-COOH DMSO solution into Milli-Q water, allowing it to oscillate for a while, and then immediately adding an aqueous DOX solution (10% of molar TPE concentration) and allowing it to oscillate again.

HPLC Analysis. HPLC analysis of all compounds was performed on a SunFire C18 analytical column (150 mm × 4.6 mm, 5 μm, Waters) with a mobile phase gradient which varied from 5% to 95% acetonitrile (the water fraction varied from 95% to 5% accordingly). The flow speed was set to 1 mL/min, and the whole gradient procedure lasted for 45 min. The UV absorbance was set at 330 nm (for TPE) and 477 nm (for DOX).

Cell Culture. The human breast cancer cell line MCF-7 was purchased from the American Type Culture Collection (ATCC; Manassas, VA). Cell culture medium and fetal bovine serum were from Wisent, Inc. (Multicell, Wisent, Inc., St. Bruno, Quebec, Canada). Trypsin-EDTA (0.25%) and antibiotic solution (penicillin and streptomycin) were purchased from Invitrogen (Invitrogen, Carlsbad, CA). Petri dishes and culture flasks were from Corning (New York). MCF-7 cells were maintained in Dulbecco's Modified Eagle's Medium (DMEM) with 10% fetal bovine serum and 1% antibiotic solution. All cells were cultured in a humidified atmosphere containing 5% CO_2 at 37 °C.

Evaluation of Cell Viability by MTT Assay. MCF-7 cells were seeded at 5×10^3 cells per well in a 96-well plate, preincubated for 24 h, and then incubated with free DOX, TCa NPs, THy NPs, THyD NPs, or TAmD NPs for 24 h at DOX concentrations ranging from 0.1 to 10 μM. The medium was then replaced with 100 μL of fresh medium containing 0.5 mg/mL of MTT, and after 2 h the MTT solution was replaced with 150 μL of DMSO solution. The absorbance was measured at 570 nm with a reference wavelength of 630 nm using an Infinite M200 microplate reader (Tecan, Durham, NC). Untreated cells in medium were used as controls.

Intracellular Distribution Analysis of THyD and TAmD NPs. MCF-7 cells (10^5) were seeded into 35 mm microscopy dishes, incubated at 37 °C for 24 h, and then incubated with 40 μM THyD or TAmD NPs for 5, 30, and 180 min at 37 °C. Cells were then rinsed with PBS twice and incubated with LysoTracker Deep Red (1000 times dilution in PBS) for lysosome staining. After 10 min incubation, cells were rinsed with PBS twice and imaged using a confocal laser scanning microscopy (CLSM, LSM710, Carl Zeiss) with excitation at 405 nm for TPE, 488 nm for DOX, and 630 nm for LysoTracker Deep Red.

Real-Time Evaluation of Drug Release. MCF-7 cells (10^5) were seeded into 35 mm microscopy dishes and incubated at 37 °C for 24 h. Before real-time CLSM observation, the medium was removed and replaced with 2 mL of fresh medium (DMEM with no Phenol Red) containing 50 μM THyD NPs or 10 μM free DOX. The microscopy dish was immediately fixed onto the observation platform of the CLSM instrument, which provided a steady CO_2 stream and a temperature of 37 °C, and images were continuously acquired with a PerkinElmer UltraVIEW spinning disk confocal system. The variations in fluorescence in the microscopy dish were captured once every 3 min. To observe the distribution of THyD NPs, the shooting duration was 150 min, and 51 pictures were obtained. For free DOX, due to the fast cell penetration and high cytotoxicity of DOX, the shooting time was reduced to 60 min, and 21 pictures were captured. To examine the cellular uptake of TPE, the excitation filter was set to 405 nm, and the emission filter was set to 450 nm. To examine DOX fluorescence, the excitation filter was 488 nm, and the emission filter was 505 nm.

Conflict of Interest: The authors declare no competing financial interest.

Supporting Information Available: Materials and methods, including the detailed experimental procedures for the synthesis and characterizations of the prodrug, as well as the control experiments *in vitro*; the detailed movies displaying the drug release process. This material is available free of charge *via* the Internet at http://pubs.acs.org.

Acknowledgment. This work was supported by the Chinese Natural Science Foundation project (81171455, 31170873), National Distinguished Young Scholars grant (31225009) from the National Natural Science Foundation of China, National Key Basic Research Program of China (2009CB930200), Chinese Academy of Sciences (CAS) "Hundred Talents Program" (07165111ZX), CAS Knowledge Innovation Program and State High-Tech Development Plan (2012AA020804, 2012AA022502 and SS2014AA020708). The authors also appreciate the support by the external cooperation program of BIC, Chinese Academy of Science, Grant No. 121D11KYSB20130006 and the "Strategic Priority Research Program" of the Chinese Academy of Sciences Grant No. XDA09030301. X.L. and G.Z. planned and supervised this research. X.X. and S.J. designed the experiments and performed the research. C.Z. provided some novel advice to the research, K.Y. cultured the cells. S.H. conducted TEM operations. F.C. provided technical helps for the CLSM operation. X.X. and S.J. contributed equally.

REFERENCES AND NOTES

1. Caldorera-Moore, M. E.; Liechty, W. B.; Peppas, N. A. Responsive Theranostic Systems: Integration of Diagnostic Imaging Agents and Responsive Controlled Release Drug Delivery Carriers. *Acc. Chem. Res.* **2011**, *44*, 1061–1070.
2. Colson, Y. L.; Grinstaff, M. W. Biologically Responsive Polymeric Nanoparticles for Drug Delivery. *Adv. Mater.* **2012**, *24*, 3878–3886.
3. Hoare, T.; Timko, B. P.; Santamaria, J.; Goya, G. F.; Irusta, S.; Lau, S.; Stefanescu, C. F.; Lin, D.; Langer, R.; Kohane, D. S. Magnetically Triggered Nanocomposite Membranes: A Versatile Platform for Triggered Drug Release. *Nano Lett.* **2011**, *11*, 1395–1400.
4. Ma, N.; Li, Y.; Xu, H.; Wang, Z.; Zhang, X. Dual Redox Responsive Assemblies Formed from Diselenide Block Copolymers. *J. Am. Chem. Soc.* **2009**, *132*, 442–443.
5. Schmidt, D. J.; Moskowitz, J. S.; Hammond, P. T. Electrically Triggered Release of a Small Molecule Drug from a Polyelectrolyte Multilayer Coating. *Chem. Mater.* **2010**, *22*, 6416–6425.
6. Moitra, P.; Kumar, K.; Kondaiah, P.; Bhattacharya, S. Efficacious Anticancer Drug Delivery Mediated by a pH-Sensitive Self-Assembly of a Conserved Tripeptide Derived from Tyrosine Kinase NGF Receptor. *Angew. Chem., Int. Ed.* **2014**, *53*, 1113–1117.
7. Wang, Y.; Zhou, K.; Huang, G.; Hensley, C.; Huang, X.; Ma, X.; Zhao, T.; Sumer, B. D.; DeBerardinis, R. J.; Gao, J. A Nanoparticle-Based Strategy for the Imaging of a Broad Range of Tumours by Nonlinear Amplification of Microenvironment Signals. *Nat. Mater.* **2014**, *13*, 204–212.
8. Wu, X.; Sun, X.; Guo, Z.; Tang, J.; Shen, Y.; James, T. D.; Tian, H.; Zhu, W. *In Vivo* and *in Situ* Tracking Cancer Chemotherapy by Highly Photostable NIR Fluorescent Theranostic Prodrug. *J. Am. Chem. Soc.* **2014**, *136*, 3579–3588.
9. Wei, T.; Liu, J.; Ma, H.; Cheng, Q.; Huang, Y.; Zhao, J.; Huo, S.; Xue, X.; Liang, Z.; Liang, X.-J. Functionalized Nanoscale Micelles Improve Drug Delivery for Cancer Therapy *in Vitro* and *in Vivo*. *Nano Lett.* **2013**, *13*, 2528–2534.
10. Yuan, L.; Lin, W.; Zheng, K.; Zhu, S. FRET-Based Small-Molecule Fluorescent Probes: Rational Design and Bioimaging Applications. *Acc. Chem. Res.* **2013**, *46*, 1462–1473.
11. Chen, L.; Li, J.; Du, L.; Li, M. Strategies in the Design of Small-Molecule Fluorescent Probes for Peptidases. *Med. Res. Rev.* **2014**, *34*, 1217–124.
12. Kobayashi, H.; Ogawa, M.; Alford, R.; Choyke, P. L.; Urano, Y. New Strategies for Fluorescent Probe Design in Medical Diagnostic Imaging. *Chem. Rev.* **2009**, *110*, 2620–2640.
13. Yang, J.; Chen, H.; Vlahov, I. R.; Cheng, J.-X.; Low, P. S. Evaluation of disulfide reduction during receptor-mediated endocytosis by using FRET imaging. *Proc. Natl. Acad. Sci. U.S.A.* **2006**, *103*, 13872–13877.
14. Lai, J.; Shah, B. P.; Garfunkel, E.; Lee, K.-B. Versatile Fluorescence Resonance Energy Transfer-Based Mesoporous Silica Nanoparticles for Real-Time Monitoring of Drug Release. *ACS Nano* **2013**, *7*, 2741–2750.
15. Wang, R.; Yu, F.; Chen, L.; Chen, H.; Wang, L.; Zhang, W. A Highly Selective Turn-On Near-Infrared Fluorescent Probe for Hydrogen Sulfide Detection and Imaging in Living Cells. *Chem. Commun.* **2012**, *48*, 11757–11759.
16. Wang, R.; Yu, F.; Liu, P.; Chen, L. A Turn-On Fluorescent Probe Based on Hydroxylamine Oxidation for Detecting Ferric Ion Selectively in Living Cells. *Chem. Commun.* **2012**, *48*, 5310–5312.
17. Lim, S.-Y.; Hong, K.-H.; Kim, D. I.; Kwon, H.; Kim, H.-J. Tunable Heptamethine−Azo Dye Conjugate as an NIR Fluorescent Probe for the Selective Detection of Mitochondrial Glutathione over Cysteine and Homocysteine. *J. Am. Chem. Soc.* **2014**, *136*, 7018–7025.

18. Yang, G.; Cao, L.; Li, X.; Wang, S.; Li, S.; Li, Y. Novel Nanogel-based Fluorescent Probe for Ratiometric Detection of Intracellular pH Values. *Chem. Commun.* **2014**, *50*, 8787–8790.
19. Hettiarachchi, S. U.; Prasai, B.; McCarley, R. L. Detection and Cellular Imaging of Human Cancer Enzyme Using a Turn-On, Wavelength-Shiftable, Self-Immolative Profluorophore. *J. Am. Chem. Soc.* **2014**, *136*, 7575–7578.
20. Kim, H. J.; Heo, C. H.; Kim, H. M. Benzimidazole-Based Ratiometric Two-Photon Fluorescent Probes for Acidic pH in Live Cells and Tissues. *J. Am. Chem. Soc.* **2013**, *135*, 17969–17977.
21. Zhao, Y.-X.; Hua, H.-Y.; Chang, M.; Liu, W.-J.; Zhao, Y.; Liu, H.-M. Preparation and Cytotoxic Activity of Hydroxycamptothecin Nanosuspensions. *Int. J. Pharm.* **2010**, *392*, 64–71.
22. Kasai, H.; Murakami, T.; Ikuta, Y.; Koseki, Y.; Baba, K.; Oikawa, H.; Nakanishi, H.; Okada, M.; Shoji, M.; Ueda, M.; et al. Creation of Pure Nanodrugs and Their Anticancer Properties. *Angew. Chem., Int. Ed.* **2012**, *51*, 10315–10318.
23. Li, X.; Hirsh, D. J.; Cabral-Lilly, D.; Zirkel, A.; Gruner, S. M.; Janoff, A. S.; Perkins, W. R. Doxorubicin Physical State in Solution and inside Liposomes Loaded *via* a pH Gradient. *BBA-Biomembranes* **1998**, *1415*, 23–40.
24. Liu, S.; Zhou, G.; Liu, D.; Xie, Z.; Huang, Y.; Wang, X.; Wu, W.; Jing, X. Inhibition of Orthotopic Secondary Hepatic Carcinoma in Mice by Doxorubicin-Loaded Electrospun Polylactide Nanofibers. *J. Mater. Chem. B* **2013**, *1*, 101–109.
25. Thomas, S. W.; Joly, G. D.; Swager, T. M. Chemical Sensors Based on Amplifying Fluorescent Conjugated Polymers. *Chem. Rev.* **2007**, *107*, 1339–1386.
26. Hong, Y.; Lam, J. W. Y.; Tang, B. Z. Aggregation-induced emission: phenomenon, mechanism and applications. *Chem. Commun.* **2009**, 4332–4353.
27. Chen, C.-T. Evolution of Red Organic Light-Emitting Diodes: Materials and Devices. *Chem. Mater.* **2004**, *16*, 4389–4400.
28. Yu, Y.; Feng, C.; Hong, Y.; Liu, J.; Chen, S.; Ng, K. M.; Luo, K. Q.; Tang, B. Z. Cytophilic Fluorescent Bioprobes for Long-Term Cell Tracking. *Adv. Mater.* **2011**, *23*, 3298–3302.
29. Li, K.; Zhu, Z.; Cai, P.; Liu, R.; Tomczak, N.; Ding, D.; Liu, J.; Qin, W.; Zhao, Z.; Hu, Y.; et al. Organic Dots with Aggregation-Induced Emission (AIE Dots) Characteristics for Dual-Color Cell Tracing. *Chem. Mater.* **2013**, *25*, 4181–4187.
30. Wang, Z.; Chen, S.; Lam, J. W. Y.; Qin, W.; Kwok, R. T. K.; Xie, N.; Hu, Q.; Tang, B. Z. Long-Term Fluorescent Cellular Tracing by the Aggregates of AIE Bioconjugates. *J. Am. Chem. Soc.* **2013**, *135*, 8238–8245.
31. Wang, J.; Mei, J.; Hu, R.; Sun, J. Z.; Qin, A.; Tang, B. Z. Click Synthesis, Aggregation-Induced Emission, E/Z Isomerization, Self-Organization, and Multiple Chromisms of Pure Stereoisomers of a Tetraphenylethene-Cored Luminogen. *J. Am. Chem. Soc.* **2012**, *134*, 9956–9966.
32. Hong, Y.; Lam, J. W. Y.; Tang, B. Z. Aggregation-Induced Emission. *Chem. Soc. Rev.* **2011**, *40*, 5361–5388.
33. Xue, X.; Zhao, Y.; Dai, L.; Zhang, X.; Hao, X.; Zhang, C.; Huo, S.; Liu, J.; Liu, C.; Kumar, A.; et al. Spatiotemporal Drug Release Visualized through a Drug Delivery System with Tunable Aggregation-Induced Emission. *Adv. Mater.* **2014**, *26*, 712–717.
34. Wang, F.; Wang, Y.-C.; Dou, S.; Xiong, M.-H.; Sun, T.-M.; Wang, J. Doxorubicin-Tethered Responsive Gold Nanoparticles Facilitate Intracellular Drug Delivery for Overcoming Multidrug Resistance in Cancer Cells. *ACS Nano* **2011**, *5*, 3679–3692.
35. Du, J.-Z.; Du, X.-J.; Mao, C.-Q.; Wang, J. Tailor-Made Dual pH-Sensitive Polymer–Doxorubicin Nanoparticles for Efficient Anticancer Drug Delivery. *J. Am. Chem. Soc.* **2011**, *133*, 17560–17563.
36. Zhang, C.; Liu, C.; Xue, X.; Zhang, X.; Huo, S.; Jiang, Y.; Chen, W.-Q.; Zou, G.; Liang, X.-J. Salt-Responsive Self-Assembly of Luminescent Hydrogel with Intrinsic Gelation-Enhanced Emission. *ACS Appl. Mater. Interfaces* **2013**, *6*, 757–762.
37. Melhuish, W. H. Quantum Efficiencies of Fluorescence of Organic Substances: Effect of Solvent and Concentration of the Fluorescent Solute. *J. Phys. Chem.* **1961**, *65*, 229–235.
38. Fletcher, A. N. Quinine Sulfate as a Fluorescence Quantum Yield Standard. *Photochem. Photobiol.* **1969**, *9*, 439–444.
39. Zhang, C.; Jin, S.; Li, S.; Xue, X.; Liu, J.; Huang, Y.; Jiang, Y.; Chen, W.-Q.; Zou, G.; Liang, X.-J. Imaging Intracellular Anti-Cancer Drug Delivery by Self-Assembly Micelles with Aggregation-Induced Emission (AIE Micelles). *ACS Appl. Mater. Interfaces* **2014**, *6*, 5212–5220.
40. Appelqvist, H.; Wäster, P.; Kågedal, K.; Öllinger, K. The Lysosome: from Waste Bag to Potential Therapeutic Target. *J. Mol. Cell Biol.* **2013**, *5*, 214–226.
41. de Duve, C.; Wattiaux, R. Functions of Lysosomes. *Annu. Rev. Physiol.* **1966**, *28*, 435–492.
42. Mohan, P.; Rapoport, N. Doxorubicin as a Molecular Nanotheranostic Agent: Effect of Doxorubicin Encapsulation in Micelles or Nanoemulsions on the Ultrasound-Mediated Intracellular Delivery and Nuclear Trafficking. *Mol. Pharmaceutics* **2010**, *7*, 1959–1973.
43. Nel, A. E.; Madler, L.; Velegol, D.; Xia, T.; Hoek, E. M. V.; Somasundaran, P.; Klaessig, F.; Castranova, V.; Thompson, M. Understanding Biophysicochemical Interactions at the Nano-Bio Interface. *Nat. Mater.* **2009**, *8*, 543–557.
44. Davis, M. E.; Chen, Z.; Shin, D. M. Nanoparticle Therapeutics: an Emerging Treatment Modality for Cancer. *Nat. Rev. Drug Discovery* **2008**, *7*, 771–782.
45. Panyam, J.; Labhasetwar, V. Biodegradable Nanoparticles for Drug and Gene Delivery to Cells and Tissue. *Adv. Drug Deliver. Rev.* **2003**, *55*, 329–347.